Next Materials 7 (2025) 100440

Contents lists available at ScienceDirect

Next Materials

journal homepage: www.sciencedirect.com/journal/next-materials

Research article

Role of molecular packing in RTP features of positional isomers: The case study of triimidazo-triazine functionalized with ethynyl pyridine moieties

Daniele Malpicci [a,b], Stefano Di Ciolo [a], Elena Cariati [a,b,c,*], Elena Lucenti [b,c], Daniele Marinotto [b,c], Daniele Maver [a,b], Clelia Giannini [a,**], Lucia Carlucci [a], Chiara Botta [d], Alessandra Forni [b,c,***]

[a] Department of Chemistry, Università degli Studi di Milano, via Golgi 19, Milano 20133, Italy
[b] Institute of Chemical Sciences and Technologies "Giulio Natta" (SCITEC) of CNR, via Golgi 19, Milano 20133, Italy
[c] INSTM Research Unit of Milano, via Golgi 19, Milano 20133, Italy
[d] Institute of Chemical Sciences and Technologies "Giulio Natta" (SCITEC) of CNR, via Corti 12, Milano 20133, Italy

ARTICLE INFO

Keywords:
Excitation dependent luminescence
Organic room temperature phosphorescence
Aggregation induced enhanced emission
Supramolecular interactions
Nitrogen rich aromatic compounds

ABSTRACT

Organic materials characterized by multi-component emissive behavior including RTP features are extremely desirable for various applications. Frequently, long lasting emissions of solids are originated from intermolecular interactions whose role is far from being fully understood. In this context, positional isomers with similar molecular properties but different packing arrangement can be a useful tool to get a deeper comprehension of the mechanisms involved in the solid state emissive behavior. Here, the results obtained on two derivatives of cyclic triimidazole (**TT**) functionalized with a pyridin-2-yl or 4-yl ethynyl group are presented and interpreted through spectroscopical, structural and computational studies. The two isomers are hardly emissive in solution but become good emitters in blended PMMA films displaying almost overlapping fluorescence and phosphorescence. In solid-state, two additional lower energy phosphorescences are activated through the establishment of either π-π stacking or synergic π-π/hydrogen bond interactions. Stronger aggregated RTP features are observed in the pyridin-2-ylethynyl derivative which displays tighter π-π stacking interactions.

1. Introduction

Purely organic materials showing Room Temperature Phosphorescence (RTP) have attracted attention in the last decade owing to the benefits they offer, including biocompatibility and low cost, compared to the widely used phosphorescent inorganic materials. Organic RTP applications in several fields such as bioimaging [1–4], anti-counterfeiting [5–13], catalysis [14] and displays [15–17] are emerging. However, the development of organic RTP materials is hampered by intrinsic drawbacks such as weak spin–orbit coupling (SOC) and slow radiative decay rates of triplet excitons.

Different strategies have been developed to realize organic RTP materials spanning from molecular engineering, specifically addressed to enhance SOC and reduce the singlet-triplet energy gap [18–22], to proper supramolecular organization based for example on H-aggregation [23–25], host–guest systems [26–32] and halogen bonding [33–35]. The role of intermolecular interactions can be efficaciously investigated in polymorphs where differences in photophysical properties are only related to supramolecular features [36–44]. Otherwise, structural isomers with similar molecular properties, for example positional isomers, but different packing arrangement can be a useful tool, even if less explored than polymorphism, to deepen the mechanism involved in the solid-state optical behavior [45,46].

In this context, triimidazo[1,2-*a*:1',2'-*c*:1'',2''-*e*][1,3,5]triazine, **TT**, has revealed as an interesting long lasting (more than 1 s) RTP system whose emissive properties have been related to the strong interchromophoric π-π stacking interactions present in its crystals [47]. In agreement with this interpretation, its positional isomer, namely triimidazo[1,2-*a*:1',2'-*c*:1'',5''-*e*][1,3,5]triazine, having weaker stacking interactions, does not display ultralong emission.

* Corresponding author at: Department of Chemistry, Università degli Studi di Milano, via Golgi 19, Milano 20133, Italy.
** Corresponding author.
*** Corresponding author at: Institute of Chemical Sciences and Technologies "Giulio Natta" (SCITEC) of CNR, via Golgi 19, Milano 20133, Italy.
E-mail addresses: elena.cariati@unimi.it (E. Cariati), clelia.giannini@unimi.it (C. Giannini), alessandra.forni@scitec.cnr.it (A. Forni).

https://doi.org/10.1016/j.nxmate.2024.100440
Received 9 October 2024; Received in revised form 22 November 2024; Accepted 25 November 2024

Starting from the **TT**-scaffold, in the last few years, many **TTs** have been prepared revealing to be not only interesting RTP materials but also ligands for the construction of photoluminescent complexes and coordination polymers [48–60]. One peculiar feature of many **TTs** is an excitation dependent PL (photoluminescent) behavior comprising short and long-lived molecular and supramolecular emissions, these latter clearly related to intermolecular interactions and therefore affected by crystallinity degree, solution concentration and matrix loading.

Intriguingly, some **TTs** have been isolated as different polymorphs or solvated/desolvated forms, allowing to better investigate the effect of solid-state chromophore organization on the emissive properties. For example, in the case of 3-(pyridin-2-yl)triimidazotriazine, *i.e.* the pyridine derivative whose nitrogen atom is located in the ortho position with respect to **TT**, three polymorphs have been isolated [55]. The three forms display dual fluorescence and dual phosphorescence all of molecular origin. Moreover, additional low energy supramolecular phosphorescences have been disclosed with features varying with the polymorph crystal structure and therefore associated with its specific π-π columnar or dimeric aggregate. Two polymorphs have also been obtained for carbazole-functionalized **TT** with the two units connected through a C-N bond (3-(9*H*-carbazol-9-yl)triimidazo[1,2-*a*:1',2'-*c*:1'',2''-*e*][1,3,5]triazine, **TT-(N)-Cz**) [56]. Both polymorphs are characterized by π-π stacking interactions between **TT** moieties and show dual fluorescence and dual phosphorescence. The high energy fluorescence and phosphorescence have been assigned to molecular excited states of Cz character, while the lower energy ones to π-π (**TT-TT**) aggregates. In agreement, the polymorph with stronger π-π interactions revealed more intense supramolecular contributions which can be attenuated through grinding [56].

Here, we report the synthesis, characterization and full photophysical investigation through experimental and computational analysis of two new **TTs** positional isomers, namely 3-(pyridin-2-ylethynyl)triimidazo[1,2-*a*:1',2'-*c*:1'',2''-*e*][1,3,5]triazine, **TT-E-2Py** and 3-(pyridin-4-ylethynyl)triimidazo[1,2-*a*:1',2'-*c*:1'',2''-*e*][1,3,5]triazine, **TT-E-4Py**. The two compounds possess very similar optical features at molecular level but subtly different packing arrangements reflecting in rather dissimilar solid state photophysical behavior comprising one fluorescence and three phosphorescences of molecular and supramolecular origins. In particular, tighter π-π stacking interactions of **TT-E-2Py**, as determined by single crystal X-ray diffraction studies, reflect in its stronger aggregated RTP features. On the other side, H-bonded chains (in **TT-E-2Py**) and dimers (in **TT-E-4Py**) of π-π aggregates are suggested to be responsible for a common low energy phosphorescence recognizable only in delayed spectra. This investigation therefore represents an additional step forward in the knowledge of the effect of chromophore organization on the related photophysics.

2. Methods

2.1. General information

All reagents and model molecules were purchased from chemical suppliers and used without further purification unless otherwise stated. **TT-E-2Py** and **TT-E-4Py** have been prepared by Sonogashira cross-coupling (see Scheme 1) between commercially available 2-ethynylpyridine or 4-ethynylpyridine and 3-bromotriimidazo[1,2-*a*:1',2'-*c*:1'',2''-*e*][1,3,5]triazine **TT-Br**, synthetized according to literature procedures [53,61]. Thin layer chromatography (TLC) was performed using Merck silica gel 60 F254 precoated plates. Column chromatography was carried out by using Merck 60 silica gel.

^{1}H and ^{13}C NMR spectra were recorded at 300 K on a Bruker AVANCE-400 instrument (400 MHz). Chemical shifts are reported in parts per million (ppm) and are referenced to the residual solvent peak (CD_2Cl_2, ^{1}H: δ = 5.32 ppm, ^{13}C: δ = 54.0 ppm). Coupling constants (J) are given in hertz (Hz) and are quoted to the nearest 0.5 Hz. Peak multiplicities are described in the following way: s, singlet; d, doublet; t, triplet; m, multiplet.

Polymethylmethacrylate (PMMA) films were prepared by spin coating (2000 rpm, 60 s) a dichloromethane (DCM) solution of the chromophore on a quartz substrate (chromophore/PMMA = 0.5, 1 and 4 wt%; PMMA = 10 wt% with respect to the solvent).

Mass spectra were recorded on a Thermo Fisher LCQ Fleet Ion Trap Mass Spectrometer equipped with UltiMate™ 3000 high-performance liquid chromatography (HPLC) system.

2.2. Synthesis of 3-(pyridin-2-ylethynyl)triimidazo*[1,2-a:1',2'-c:1'',2''-e]*[1,3,5]triazine (TT-E-2Py)

A 50 mL dry Schlenk flask equipped with a magnetic stirrer under Ar atmosphere was loaded in the following order with: **TT-Br** (0.200 g; 0.722 mmol), $Pd(PPh_3)_2Cl_2$ (0.025 g, 0.036 mmol), dry *N*,*N*-diisopropylethylamine (DIPEA, 1 mL), dry *N*,*N*-dimethylformamide (DMF, 10 mL) and 2-ethynylpyridine (0.146 mL; 1.44 mmol). The flask was heated under static Ar atmosphere at 393 K for 16 h. The resulting brown reaction mixture was then cooled to room temperature and evaporated to dryness. The crude reaction mixture was purified by gravimetric chromatography on SiO_2 with DCM/Acetonitrile (ACN) as eluents (R_f = 0.35 in DCM/ACN = 9:1). Further crystallization by slowly cooling to room temperature a boiling ACN solution of **TT-E-2Py** afforded the product as a white solid (0.080 g, 0.267 mmol, Yield: 37 %.).

^{1}H NMR (400 MHz, CD_2Cl_2, 298 K, ppm): δ 8.64 (d, *J* = 4.8 Hz, 1H), 7.84 (d, *J* = 1.54 Hz, 1H), 7.81 (d, *J* = 1.57 Hz, 1H), 7.77 (dt, *J* = 7.70, 1.59 Hz 1H), 7.71 (d, *J* = 7.7 Hz, 1H), (7.60, s, 1H), 7,39 (d, *J* = 1.57 Hz, 1H), 7,32 (t, *J* = 6.16 Hz, 1H), 7,29 (d, *J* = 1.54 Hz, 1H).

^{13}C NMR (100 MHz, CD_2Cl_2, 298 K, ppm): 150.8 (CH); 143.2 (C); 136.8 (CH); 136.0 (C); 135.9 (C); 135.5 (C); 129.9 (CH); 129.9 (CH); 127.9 (CH); 123.9 (CH); 112.2 (CH); 112.0 (CH); 110.4 (C); 97.1 (C); 76.4 (C).

ESI-MS: m/z 300 $[M + H]^+$.

2.3. Synthesis of 3-(pyridin-4-ylethynyl)triimidazo*[1,2-a:1',2'-c:1'',2''-e]*[1,3,5]triazine (TT-E-4Py)

A 50 mL dry Schlenk flask equipped with a magnetic stirrer under Ar atmosphere was loaded in the following order with: **TT-Br** (0.200 g; 0.722 mmol), $Pd(PPh_3)_2Cl_2$ (0.025 g, 0.036 mmol), dry DIPEA (1 mL), dry DMF(10 mL) and 4-ethynylpyridine (0.146 mL; 1.44 mmol). The flask was heated under Ar atmosphere at 393 K for 16 h. The resulting brown reaction mixture was then cooled to room temperature and evaporated to dryness. The crude reaction mixture was purified by gravimetric chromatography on SiO_2 with DCM/ACN as eluents (R_f = 0.35 in DCM/2-propanol = 8:2). Further precipitation from ACN gave the **TT-E-4Py** product as a white solid (0.090 g, 0.30 mmol, Yield:

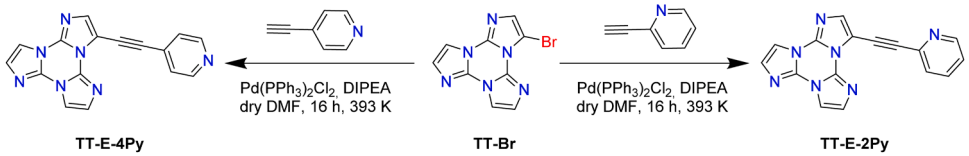

Scheme 1. Synthesis of **TT-E-2Py** (right) and **TT-E-4Py** (left).

40 %.).

^{1}H NMR (400 MHz, CD_2Cl_2, 298 K, ppm): δ 8.64 (m, 2H), 7.84 (d, J = 1.66 Hz, 1H), 7.81 (d, J = 1.71 Hz, 1H), (7.56, s, 1H), 7,51 (m, 2H), 7,37 (d, J = 1.66 Hz, 1H), 7,28 (d, J = 1.71 Hz, 1H).

^{13}C NMR (100 MHz, CD_2Cl_2, 298 K, ppm): 150.5 (CH); 136.1 (C), 135.7 (CH), 135.7 (C), 135.6 (C), 130.9 (C), 130.0 (CH), 129.9 (CH), 125.4 (CH), 112.2 (CH), 112.0 (CH), 110.3 (C), 95.4 (C), 81.3 (C).

ESI-MS: m/z 300 $[M + H]^+$.

3. Results and discussion

TT-E-2Py and **TT-E-4Py** have been prepared by Sonogashira cross-coupling between **TT-Br** and commercially available 2-ethynylpyridine or 4-ethynylpyridine, respectively (Scheme 1). The products have been purified by standard chromatography techniques and characterized by NMR spectroscopy, mass spectrometry and X-ray analysis (see Experimental and Supporting information Sections). Before performing their photophysical characterization, the compounds were recrystallized several times in order to avoid signals due to impurities which are particularly detrimental in the solid state. Different batches of the compounds displayed perfectly matching absorption and emission spectra.

Diluted solutions of **TT-E-xPy** (x equal to 2 or 4) in DMSO (5×10^{-6} M) display superimposable absorption and emission spectra. A high energy broad signal (at 319 nm) and a narrow, weaker one (333 nm) are present in the absorption spectrum of the two compounds while a hardly discernible broad emission at about 450 nm (weaker than the Raman signal of the solvent at 328 nm, see Figs. S7 and S8) is observed for both. To better determine the molecular behavior of the two compounds taking advantage of the rigidity of the medium, which can inhibit competitive non-radiative deactivation channels, we prepared and characterized blended thin films of **TT-E-xPy** in PMMA with low chromophore loading (w/w **TT-E-xPy**/PMMA 0.5 %, Table 1). Again, the two compounds display similar optical behavior (Figs. 1, S9 and S13), comprising two absorption peaks (at 317 and 331 nm, see Fig. 1-left where the absorption spectrum of blended film of **TT-E-2Py** is reported) and excitation dependent emissions. Specifically, by exciting at high energy (below 300 nm) an intense broad fluorescence at about 360 nm (τ_{av} = 0.55 and 0.65 ns, Figs. S10 and S14, overall Φ = 6.4 and 24.4 %, for **TT-E-2Py** and **TT-E-4Py**, respectively) dominates the spectrum. Moreover, one phosphorescence appears at about 430 nm as a shoulder (τ_{av} = 12.31 and 5.17 ms, Figs. S11 and S15, for **TT-E-2Py** and **TT-E-4Py**, respectively). This phosphorescence can be selectively activated by exciting at 360 nm, being otherwise overwhelmed by fluorescence when exciting at higher energy. However, it has to be noted that, in the case of **TT-E-2Py**, an additional weak component at 530 nm appears in the spectrum at 360 nm excitation (τ_{av} = 70.87 ms, see Fig. S12). For the two compounds, excitation profiles corresponding to fluorescence comprise two bands, approximately in the same position of the absorption spectrum, but an additional component at about 370 nm is present when monitoring the phosphorescent emission, as evident from time delayed emission spectra (see inset of Fig. 1-right). Supported by DFT/TDDFT calculations, the two high-energy (at 317 and 331 nm) bands identified in the absorption spectra of DMSO solutions and absorption/excitation spectra of blended PMMA films can be assigned to a vibronically resolved S_1 singlet state. Their 0.16 eV separation is, in fact, compatible with the stretching frequencies of C=C and C=N bonds present in both **TT-E-xPy**. Free geometry optimization of the molecules in their S_0 state leads to perfectly planar conformations with very similar S_1 levels (computed at 279 and 277 nm, with associated oscillator strengths (f) of 0.85 and 0.82 for **TT-E-2Py** and **TT-E-4Py**, respectively, see Tables S3 and S4). They correspond to (π,π*) HOMO→LUMO transitions with HOMO and LUMO delocalized on the whole molecule (Figs. S47 and S48). The poor emissive behavior of the two molecules in solution, despite the high oscillator strength of their S_1 state, could be mainly ascribed to the high conformational freedom of the molecules, which in fact are far from being planar in their crystal structures (see below). Interestingly, a (σ,π*) S_2 state involving an inner HOMO essentially localized on pyridine is computed at 246 (f = 0.003) and 250 nm (f = 0.004) for **TT-E-2Py** and **TT-E-4Py**, respectively. Owing to its symmetry, S_2 cannot be recognized in the absorption/excitation spectra, but may contribute to broaden the high energy vibronic replica of S_1. Finally, the low energy (370 nm) shoulder observed in the excitation spectra of blended PMMA films when monitoring the phosphorescent emission can be assigned to T_1, as confirmed by unrestricted DFT (UDFT) calculations on the S_0 optimized geometry, providing such state at 367 and 369 nm for **TT-E-2Py** and **TT-E-4Py**, respectively.

Table 1
Photophysical parameters of **TT-E-2Py** and **TT-E-4Py**.

	298 K			77 K	
	Φ%	**λ_{em}**	**τ_{av}**	**λ_{em}**	**τ_{av}**
TT-E-2Py					
PMMA (0.5 w/w%)	6.4	360	0.55 ns		
		430	12.31 ms		
		500	70.87 ms		
Crystals	7.6	393	1.49 ns	400	2.81 ns
		432, 461	20.7 ms	430	246 ms
		545, 586	129.6 ms	485, 524, 544, 569	410 ms
		620	21.4 ms[a]		
Ground crystals	10.3	380	1.62 ns	400	2.04 ns
		483	8.72 ms	445	11.27 ms
		551, 590	35.38 ms	487, 525, 547	217.73 ms
TT-E-4Py					
PMMA (0.5 w/w%)	24.4	360	0.65 ns		
		430	5.17 ms		
Crystals	6.6	408	3.13 ns	390, 410	5.56 ns
		462, 487	8.60 ms	434, 455, 490	15.74 ms
		496, 523	70.14 ms	495, 526	272.68 ms
		615	26.6 ms[a]		
Ground crystals	10.3	386	1.14 ns	400	2.97 ns
		464, 487	0.68 ms	460, 487	0.83 ms
		495, 523	14.21 ms	495, 526	317.80 ms

[a] Time gated spectra.

Single crystals suitable for X-ray diffraction studies have been obtained, for both compounds, by slowly cooling to room temperature boiling ACN solutions. **TT-E-2Py** and **TT-E-4Py** crystallize, respectively, in the monoclinic $P2_1/c$ and in the triclinic P-1 space groups. Both crystal structures contain one single molecule in the asymmetric unit with Z equal to 4 and 2, respectively (views of the two molecules with atomic labelling scheme are shown in Fig. S46). The molecules are characterized by a different reciprocal orientation of the two flat aromatic fragments, **TT** and pyridine, as indicated by the angles between their mean planes, 67.07(6)° and 37.82(5)° for **TT-E-2Py** and **TT-E-4Py**, respectively, resulting in a flatter conformation for **TT-E-4Py**.

In both crystal structures, the molecules pack with similar parallel alignment forming piles along the crystallographic **a** direction (Figs. 2 and 3). Such piles are differently translated in space according to the symmetry elements of the related space group. Their disposition, together with the different molecular conformations, result in different intermolecular interactions (π-π stacking and C−H···N hydrogen bonds, HBs). In both cases the molecules are parallel stacked along the crystallographic direction **a** with distances between triazinic centroids (Cg) equal to 5.087 and 4.682 Å for **TT-E-2Py** and **TT-E-4Py**, respectively. In the crystal structure of **TT-E-4Py**, the presence of a centre of inversion only, associated to translation, allows stacking of the molecules exclusively along this direction, while in **TT-E-2Py** the presence of the screw axes results in a herringbone packing of parallel columnar stacks along **a**

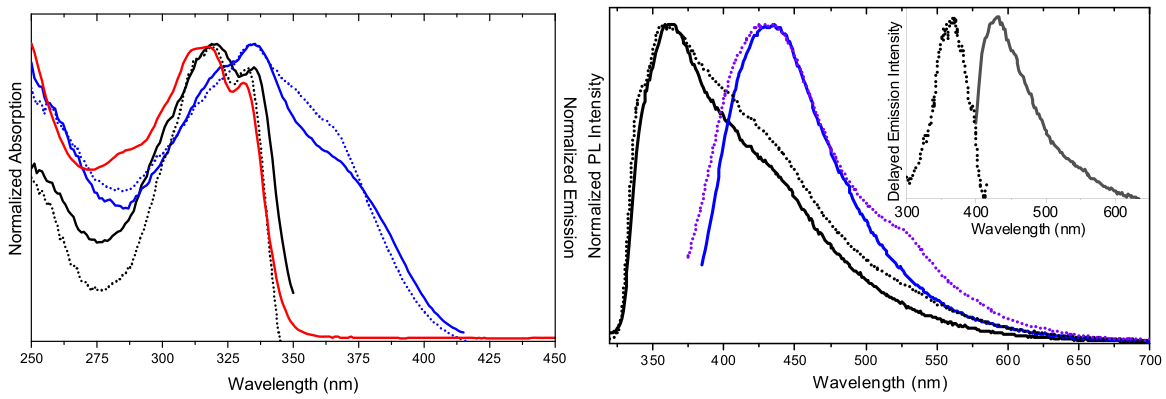

Fig. 1. **TT-E-nPy**/PMMA blended films (0.5 % w/w%) at RT. Left: normalized excitation (**TT-E-2Py**, dot lines; **TT-E-4Py**, full lines; λ_{em} = 360 nm (black); 430 nm (blue)) and absorption (**TT-E-2Py**/PMMA 4 % w/w%, red full line). Right: normalized emission (**TT-E-2Py**, dot lines; **TT-E-4Py**, full lines); λ_{exc} = 300 nm (black); 370 nm (blue). Inset: Delayed emission and excitation spectra of **TT-E-4Py**/PMMA 1 % w/w% (λ_{exc} = 370 nm, full line; λ_{em} = 430 nm, dot line; delay time 50 μs, window 100 μs).

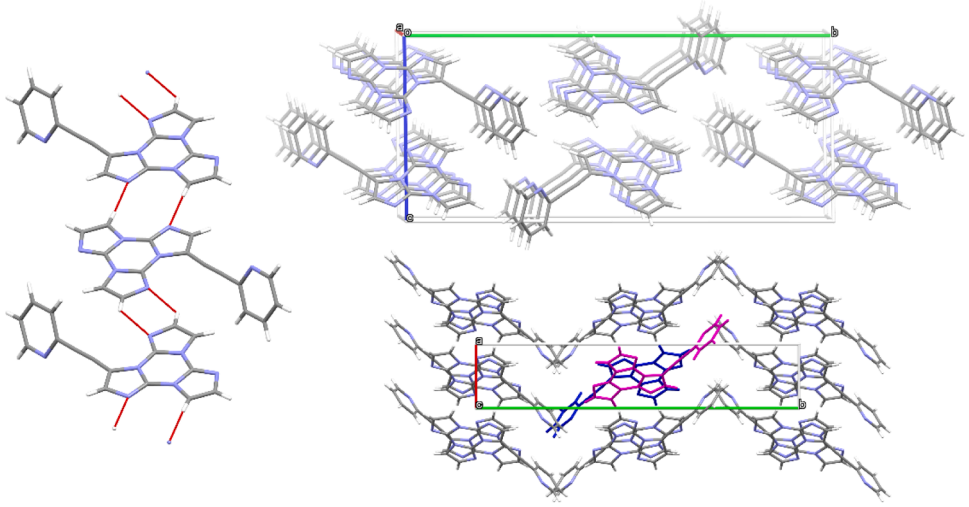

Fig. 2. Views of the crystal structure of **TT-E-2Py** showing (left) the molecular chain built up through mutual C–H···N hydrogen bonds (highlighted in red), (right up) the molecular packing approximately down the [1 0 0] direction displaying the parallel π–π stacking in the same direction and, (right bottom) the molecular packing down the [0 0 1] direction displaying the antiparallel π–π stacking of molecules.

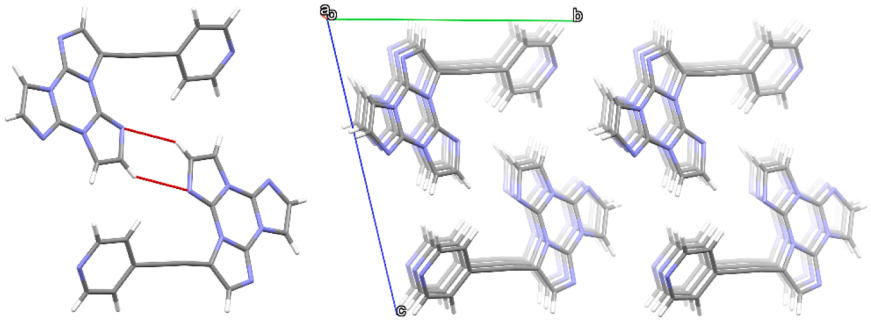

Fig. 3. Views of the crystal structure of **TT-E-4Py** showing (left) centrosymmetric dimer built up through mutual C–H···N hydrogen bonds (highlighted in red) and, (right) the molecular packing approximately down the [1 0 0] direction displaying the parallel π–π stacking in the same direction.

and antiparallel ones along **c**, the latter with Cg···Cg distances alternately equal to 5.359 and 6.101 Å. In **TT-E-2Py** each molecule interacts through mutual C–H···N(imidazole) HBs (C8–H8···N6; 3.303 and C4–H4···N2, 3.382 Å) to give chains of centrosymmetric molecules (Fig. 3-left). Moreover, the pyridyl nitrogen atom interacts with a C–H bond of a pyridyl unit belonging to a neighbouring chain (C14–H14···N7, 3.305 Å), while the N4 imidazole atom shows a long interaction with the C13–H13 pyridyl bond (C13–H13···N4, 3.457 Å) (see Table S2). In the case of **TT-E-4Py**, one of the three **TT** hexo-oriented nitrogen atoms is involved in a HB dimer through mutual C8–H8···N6 bonds (3.408 Å), a second one interacts with a pyridyl C–H bond (C13–H13···N2, 3.461 Å), while the third one (N4), as well as that

of the pyridine moiety (N7), is not involved in intermolecular interactions. The different packing of the two compounds results in more numerous and shorter HBs in **TT-E-2Py**. Overall, from comparison between the two crystal structures, it is evident that, despite similar intermolecular interactions, **TT-E-2Py** is characterized by a tighter arrangement through both C–H···N HBs and π-π stacking. The different packing was expected to reflect in the photophysical behavior of crystals of the two compounds.

In the solid state, both **TT-E-xPy** display excitation dependent and mechanochromic photoluminescent behavior which can be clearly visualized through spectra of **TT-E-xPy** crystals recorded at different excitation wavelengths before and after grinding in a mortar (Figs. 4 and 5).

By exciting at 300 nm at RT crystals of **TT-E-2Py**, a multicomponent emissive spectrum is obtained (Fig. 4-left). In particular, a high energy emission at about 393 nm with a red shifted, partially vibrationally resolved, shoulder (replicas at 432 and 461 nm) and a low energy band with replicas at 545 and 586 nm, are observed. From lifetime measurements, the high energy emission is disclosed as the convolution of one fluorescence (τ_{av} = 1.49 ns, Fig. S16) and a high energy phosphorescence (HEP, τ_{av} = 20.75 ms, Fig. S17), while the low energy component corresponds to a long-lived signal only (LEP, τ_{av} = 129.58 ms, Fig. S18). HEP and LEP appear in the PL spectrum, freed from otherwise stronger fluorescence, by exciting at sufficiently low excitation (387 nm, see Fig. 4-middle). Moreover, an additional low energy, broad contribution (red phosphorescence, RP) is disclosed only through delayed spectra. In particular, as shown in Fig. 4-middle, HEP, LEP and RP appear as a broad (at about 465 nm), a vibronically resolved (replicas at 550 and 590 nm) and a broad (at about 620 nm, τ_{av} = 21.42 ms, Fig. S19) band, respectively, in delayed spectra of crystals taken at different delay times (with RP well resolved from HEP and LEP at longer delays).

After grinding, a slight increase in the quantum yield (overall Φ = 7.6 and 10.3 % before and after grinding, respectively) is accompanied by the intensification of the fluorescence (maximum at 380 nm) with respect to the phosphorescent contributions as evidenced in PL spectra taken at 300 nm excitation (see Fig. 4-left). Concomitantly, a blue shifting towards values close to those observed for blended film (360 nm) occurs.

The PL spectrum of crystals at 77 K and 300 nm excitation (Fig. 4-right), displays vibronically resolved LEP (replicas at 485, 524, 544 and 569 nm, τ_{av} = 410 ms, Fig. S22) as major component, with fluorescence (at about 400 nm, τ_{av} = 2.81 ns, Fig. S20) and HEP (at about 430 nm, τ_{av} = 246 ms, Fig. S21) hardly recognizable. Contrarily, the high energy emissions (fluorescence and HEP) dominate the spectrum of ground crystals at 77 K (Fig. 4-right).

For what concerns crystals of **TT-E-4Py** at RT, a broad emission at 408 nm with a shoulder at about 487 nm appears in the spectrum through irradiation at 300 nm (Fig. 5-left). From lifetime measurements, the presence of one fluorescence (τ_{av} = 3.13 ns, Fig. S29) and one phosphorescence (HEP, τ_{av} = 8.60 ms, Fig. S30) is revealed. Additional long-lived contributions are recognized by their selective activation at proper excitation wavelength or through delayed spectra. In particular, two phosphorescences are observed in the PL spectrum (Fig. 5-middle): HEP at 462 and 487 nm (exciting at 390 nm) and LEP at 496 and 523 nm (at 450 nm excitation, τ_{av} = 70.14 ms, Fig. S31). Moreover, an additional low energy, broad RP is disclosed only from delayed spectra. In particular, as shown in Fig. 5-middle, delayed spectra of crystals display three phosphorescences with different temporal evolutions (see Fig. S32). HEP and LEP are better visible at short delays, while the longer lasting RP (τ_{av} = 26.6 ms, Fig. S33), with vibronic replicas at 612 and 658 nm, is well resolved from LEP at long delays.

After grinding, the slight increase in the quantum yield (overall Φ = 6.6 and 8.5 % before and after grinding, respectively) is accompanied by the intensification and a blue shifting (386 nm) of fluorescence, as supported by PL spectra taken at 300 nm excitation (Fig. 5, left).

At 77 K and 300 nm excitation (Fig. 5-right), vibronically resolved fluorescence (at 390 and 410 nm, τ_{av} = 5.56 ns, Fig. S35) and HEP (434, 455 and 490 nm, τ_{av} = 15.74 ms, Fig. S36) appear in PL spectra of crystals, while LEP (at 495 and 526 nm, τ_{av} = 272.68 ms, Fig. S37) is visible only through selective excitation at 450 nm (Fig. S34). Grinding crystals of **TT-E-4Py** (Fig. 5-right) results in much less evident effects with respect to what observed for **TT-E-2Py**. In particular, by exciting at 300 nm, fluorescence at 400 nm appears vibrationally unresolved as the only emission in the PL spectrum suggesting attenuation of HEP in its respect.

The solid-state behavior of the two compounds is therefore macroscopically different and deserves its interpretation with the aid of crystal structure analysis. In particular, by comparing the relative intensity of LEP with respect to that of the other emissions, it is evident its greater role in **TT-E-2Py** rather than **TT-E-4Py**. To be more precise, for **TT-E-2Py**, LEP is already visible in PL spectra of PMMA blended films, it becomes quite intense in crystals at RT and appears as the major component when crystals are analyzed at 77 K. After grinding, LEP is still visible but with reduced importance. On the other side, for **TT-E-4Py**, LEP is absent in blended films and it is recognizable only for crystals either in their PL spectra, both at RT and 77 K, when selectively activated or in delayed measurements, where it appears together with HEP and RP. From all these experimental observations, LEP can be unequivocally assigned to supramolecular features. After grinding, both compounds show fluorescence as prevailing component, in line with what expected for ground compounds where RTP features and, in particular, supramolecular contributions are attenuated. Based on the results of XRD studies, the greater importance of LEP in **TT-E-2Py** may be explained through its tighter packing when compared to **TT-E-4Py**, reflecting in a higher signal of the triplet exciton associated with aggregated species. The appearance of LEP in low loading blended films of **TT-E-2Py** should not be considered against its supramolecular nature, but as an additional proof of the strong tendency of this compound to give aggregated species.

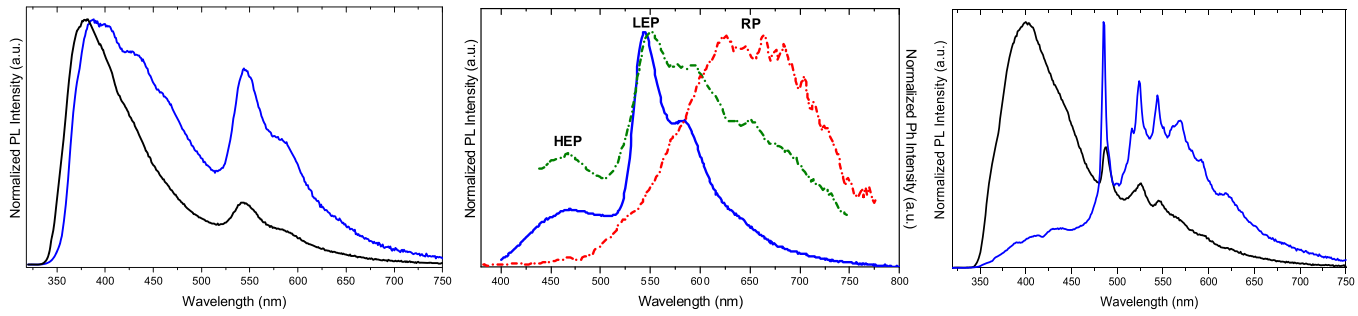

Fig. 4. Normalized spectra of **TT-E-2Py**. Left: PL at 298 K before (blue) and after (black) grinding, λ_{exc} = 300 nm. Middle: 298 K PL (blue full; λ_{exc} = 387 nm) and Ph (dash dot; λ_{exc}= 390 nm, green, delay 50 μs, window 200 μs; red, delay 200 μs, window 500 μs). Right: PL at 77 K before (blue) and after (black) grinding, λ_{exc} = 300 nm.

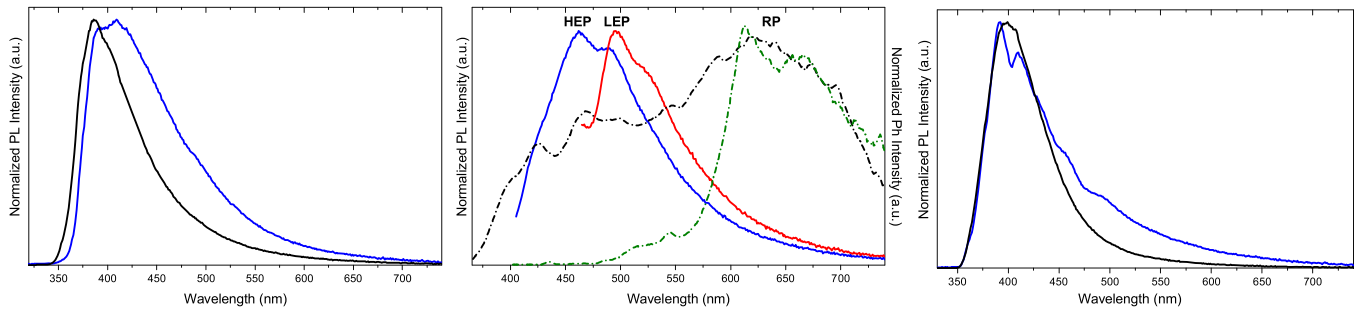

Fig. 5. Normalized spectra of **TT-E-4Py**. Left: PL at 298 K before (blue) and after (black) grinding: λ_{exc} = 300 nm. Middle: 298 K PL (full; λ_{exc} = 390 nm, blue; 450 nm, red) and Ph (dash dot; λ_{exc} = 290 nm, delay 50 μs, window 1 ms, black; 360 nm, delay 5 ms, window 10 ms, green). Right: PL at 77 K before (blue) and after (black) grinding: λ_{exc} = 300 nm.

Trickier is the interpretation of RP which appears, for both compounds, only in delayed spectra hampering a meaningful intensity comparison with the other emissions. However, its presence in crystals of both compounds suggests a common supramolecular origin. Moreover, its red shifted position with respect to LEP would indicate a more extended aggregate as responsible for its presence. Since both crystal structures are governed by π-π stacking interactions and hydrogen bonded motifs, a possible hypothesis is that, while LEP is associated with π-π aggregates within a single stack, RP can be related to π-π stacking of extended hydrogen bonded frameworks for **TT-E-2Py** and **TT-E-4Py**, respectively.

On the other side, there are no doubts regarding the molecular origin of HEP. It is present in spectra of low loaded PMMA blended films with excitation profiles matching, for both compounds, UDFT calculated T_1 which is therefore responsible for the observed phosphorescence. The PMMA matrix rigidifies the systems inhibiting molecular motions which are competitive non-radiative deactivation channels in solution. In aggregate phases, intermolecular interactions play a similar role besides protecting from oxygen quenching, altogether resulting in enhanced fast and long-lived emissive features with respect to the solution. The role of intermolecular interactions on RTP properties is emphasized through grinding experiments which result in blue shifting of the emission to values close to those observed in blended films due to the main role played by fluorescence after grinding. This effect on HEP is well disclosed in PL spectra (at 300 nm excitation) of **TT-E-4Py** which lacks LEP. In particular, at 77 K (Fig. 5-right) HEP is strongly attenuated through grinding confirming the role of particle size in rigidifying and protecting from oxygen quenching.

4. Conclusions

Two positional isomers derived from cyclic triimidazole (**TT**) functionalized with a pyridin-2-yl or 4-yl ethynyl group, **TT-E-2Py** and **TT-E-4Py**, respectively, have been synthesized and fully characterized by spectroscopic, structural and computational investigations. The two compounds are hardly emissive in solution due to the high conformational freedom. Their molecular behavior has been better disclosed in blended PMMA diluted films displaying almost overlapping emission spectra, comprising one fluorescence and a high energy phosphorescence, HEP, obviously interpreted as molecular contributions. In the solid state, two additional lower energy phosphorescences, LEP and RP, are activated in both compounds thanks to the establishment, respectively, of π-π stacking interactions and synergic π-π/hydrogen bond interactions (Fig. 6). The different packing arrangements in the crystal structures of the two compounds, with tighter π-π stacking interactions in **TT-E-2Py** with respect to **TT-E-4Py**, result in stronger aggregated RTP features in the former. In **TT-E-2Py**, in fact, LEP is quite intense in PL spectra of crystals already at RT and appears as the major component at 77 K. On the other side, for **TT-E-4Py**, LEP is recognizable for crystals either in their PL spectra only when selectively activated or in delayed

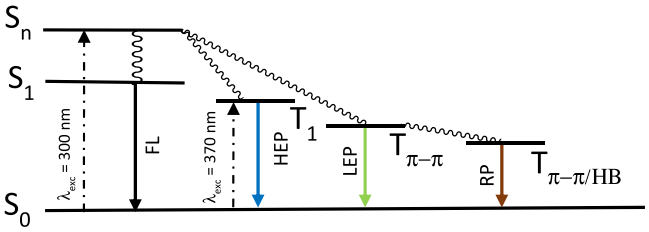

Fig. 6. Simplified Jablonski diagram for **TT-E-xPy** crystals. $T_{\pi-\pi}$ and $T_{\pi-\pi/HB}$ are triplets associated with supramolecular π-π and synergic π-π/HB aggregates, respectively.

measurements, where it appears together with HEP and RP.

Grinding experiments allow to further shed light on the role of intermolecular interactions on RTP properties of the two compounds in the solid-state. After grinding, HEP and LEP are attenuated in PL spectra of both compounds supporting the importance of crystal packing in activating LEP and in diminishing molecular motions responsible for non-radiative deactivation channels competitive with both HEP and LEP.

This investigation represents an additional step forward in the knowledge of the effect of chromophore organization on the related photophysics and further demonstrates that supramolecular assembly is an effective tool for the development of new materials with enhanced RTP properties.

Declaration of Competing Interest

The authors declare that they have no known competing financial interests or personal relationships that could have appeared to influence the work reported in this paper.

Acknowledgments

We thank Università degli Studi di Milano for financial support (PSR2022_DIP_005_PI_LCAR). The use of instrumentation purchased through the Regione Lombardia-Fondazione Cariplo joint SmartMatLab Project is gratefully acknowledged.

Appendix A. Supporting information

Supplementary data associated with this article can be found in the online version at doi:10.1016/j.nxmate.2024.100440.

References

[1] Q. Dang, Y. Jiang, J. Wang, J. Wang, Q. Zhang, M. Zhang, S. Luo, Y. Xie, K. Pu, Q. Li, Z. Li, Adv. Mater. 32 (2020) 2006752, https://doi.org/10.1002/adma.202006752.

[2] W. Qin, P. Zhang, H. Li, J.W.Y. Lam, Y. Cai, R.T.K. Kwok, J. Qian, W. Zheng, B. Z. Tang, Chem. Sci. 9 (2018) 2705–2710, https://doi.org/10.1039/C7SC04820C.
[3] Y. Wang, H. Gao, J. Yang, M. Fang, D. Ding, B.Z. Tang, Z. Li, Adv. Mater. 33 (2021) 2007811, https://doi.org/10.1002/adma.202007811.
[4] J. Zhi, Q. Zhou, H. Shi, Z. An, W. Huang, Chem. Asian J. 15 (2020) 947–957, https://doi.org/10.1002/asia.201901658.
[5] M. Cao, Y. Ren, Y. Wu, J. Shen, S. Li, Z.-Q. Yu, S. Liu, J. Li, O.J. Rojas, Z. Chen, Nat. Commun. 15 (2024) 2375, https://doi.org/10.1038/s41467-024-45844-5.
[6] L. Gu, H. Wu, H. Ma, W. Ye, W. Jia, H. Wang, H. Chen, N. Zhang, D. Wang, C. Qian, Z. An, W. Huang, Y. Zhao, Nat. Commun. 11 (2020) 944, https://doi.org/10.1038/s41467-020-14792-1.
[7] K. Jiang, Y. Wang, C. Cai, H. Lin, Adv. Mater. 30 (2018) 1800783, https://doi.org/10.1002/adma.201800783.
[8] Y. Lei, W. Dai, J. Guan, S. Guo, F. Ren, Y. Zhou, J. Shi, B. Tong, Z. Cai, J. Zheng, Y. Dong, Angew. Chem. Int. Ed. 59 (2020) 16054–16060, https://doi.org/10.1002/anie.202003585.
[9] Y. Li, P. Gao, Chemosensors 11 (2023) 489, https://doi.org/10.3390/chemosensors11090489.
[10] B. Sk, S. Hirata, Adv. Sci. (2024) 2308897, https://doi.org/10.1002/advs.202308897.
[11] Y. Su, S.Z.F. Phua, Y. Li, X. Zhou, D. Jana, G. Liu, W.Q. Lim, W.K. Ong, C. Yang, Y. Zhao, Sci. Adv. 4 (2018) eaas9732, https://doi.org/10.1126/sciadv.aas9732.
[12] J. Tan, Q. Li, S. Meng, Y. Li, J. Yang, Y. Ye, Z. Tang, S. Qu, X. Ren, Adv. Mater. 33 (2021) 2006781, https://doi.org/10.1002/adma.202006781.
[13] B. Wang, Y. Li, C. Zhang, S. Sun, W. He, D. Wang, H. Cao, Z. Yang, New J. Chem. 48 (2024) 9030–9035, https://doi.org/10.1039/D4NJ00510D.
[14] Y. Cao, D. Wang, Y. Zhang, G. Li, C. Gao, W. Li, X. Chen, X. Chen, P. Sun, Y. Dong, Z. Cai, Z. He, Angew. Chem. Int. Ed. 63 (2024) e202401331, https://doi.org/10.1002/anie.202401331.
[15] S. Hirata, K. Totani, H. Kaji, M. Vacha, T. Watanabe, C. Adachi, Adv. Opt. Mater. 1 (2013) 438–442, https://doi.org/10.1002/adom.201300136.
[16] M. Stanitska, D. Volyniuk, B. Minaev, H. Agren, J.V. Grazulevicius, J. Mater. Chem. C 12 (2024) 2662–2698, https://doi.org/10.1039/D3TC04514E.
[17] X. Yao, Y. Li, H. Shi, Z. Yu, B. Wu, Z. Zhou, C. Zhou, X. Zheng, M. Tang, X. Wang, H. Ma, Z. Meng, W. Huang, Z. An, Nat. Commun. 15 (2024) 4520, https://doi.org/10.1038/s41467-024-48856-3.
[18] Y. Tani, K. Miyata, E. Ou, Y. Oshima, M. Komura, M. Terasaki, S. Kimura, T. Ehara, K. Kubo, K. Onda, T. Ogawa, Chem. Sci. 15 (2024) 10784–10793, https://doi.org/10.1039/D4SC02841D.
[19] Z. Wang, X. Cheng, Y. Xie, S. Liu, M. Dong, J. Zhao, F. Liang, Z. An, W. Huang, CCS Chem. 5 (2023) 292–309, https://doi.org/10.31635/ccschem.022.202202242.
[20] H. Wu, D. Wang, J. Zhang, P. Alam, Z. Zhao, Y. Xiong, D. Wang, B.Z. Tang, J. Mater. Chem. C (2024), https://doi.org/10.1039/D4TC01387E.
[21] W.Z. Yuan, X.Y. Shen, H. Zhao, J.W.Y. Lam, L. Tang, P. Lu, C. Wang, Y. Liu, Z. Wang, Q. Zheng, J.Z. Sun, Y. Ma, B.Z. Tang, J. Phys. Chem. C 114 (2010) 6090–6099, https://doi.org/10.1021/jp909388y.
[22] T. Zhu, T. Yang, Q. Zhang, W.Z. Yuan, Nat. Commun. 13 (2022) 2658, https://doi.org/10.1038/s41467-022-30368-7.
[23] Y. Cao, Z. Xu, X. Zhao, Y. Yang, H. Liu, P. Wang, M. Yu, H. Li, H. Fu, Chem. Sci. 15 (2024) 13930–13936, https://doi.org/10.1039/D4SC02867H.
[24] S. Li, L. Fu, X. Xiao, H. Geng, Q. Liao, Y. Liao, H. Fu, Angew. Chem. Int. Ed. 60 (2021) 18059–18064, https://doi.org/10.1002/anie.202103192.
[25] P. Pattanayak, N. Modak, S. Guchhait, N. Ghosh, P. Purkayastha, Adv. Opt. Mater. 12 (2024) 2400404, https://doi.org/10.1002/adom.202400404.
[26] L. Bian, H. Shi, X. Wang, K. Ling, H. Ma, M. Li, Z. Cheng, C. Ma, S. Cai, Q. Wu, N. Gan, X. Xu, Z. An, W. Huang, J. Am. Chem. Soc. 140 (2018) 10734–10739, https://doi.org/10.1021/jacs.8b03867.
[27] R. Kabe, C. Adachi, Nature 550 (2017) 384–387, https://doi.org/10.1038/nature24010.
[28] D. Li, F. Lu, J. Wang, W. Hu, X.-M. Cao, X. Ma, H. Tian, J. Am. Chem. Soc. 140 (2018) 1916–1923, https://doi.org/10.1021/jacs.7b12800.
[29] X.-K. Ma, Y. Liu, Acc. Chem. Res. 54 (2021) 3403–3414, https://doi.org/10.1021/acs.accounts.1c00336.
[30] H. Mieno, R. Kabe, N. Notsuka, M.D. Allendorf, C. Adachi, Adv. Opt. Mater. 4 (2016) 1015–1021, https://doi.org/10.1002/adom.201600103.
[31] X. Zhang, L. Du, W. Zhao, Z. Zhao, Y. Xiong, X. He, P.F. Gao, P. Alam, C. Wang, Z. Li, J. Leng, J. Liu, C. Zhou, J.W.Y. Lam, D.L. Phillips, G. Zhang, B.Z. Tang, Nat. Commun. 10 (2019) 5161, https://doi.org/10.1038/s41467-019-13048-x.
[32] Z.-Y. Zhang, W.-W. Xu, W.-S. Xu, J. Niu, X.-H. Sun, Y. Liu, Angew. Chem. Int. Ed. 59 (2020) 18748–18754, https://doi.org/10.1002/anie.202008516.
[33] A. Abe, K. Goushi, M. Mamada, C. Adachi, Adv. Mater. (2023) e2211160, https://doi.org/10.1002/adma.202211160.
[34] O. Bolton, K. Lee, H.-J. Kim, K.Y. Lin, J. Kim, Nat. Chem. 3 (2011) 205–210, https://doi.org/10.1038/nchem.984.
[35] H. Shi, Z. An, P.-Z. Li, J. Yin, G. Xing, T. He, H. Chen, J. Wang, H. Sun, W. Huang, Y. Zhao, Cryst. Growth Des. 16 (2016) 808–813, https://doi.org/10.1021/acs.cgd.5b01400.
[36] J. Gao, S. Shi, Q. Li, H. Ma, Dyes Pigments 208 (2023) 110853, https://doi.org/10.1016/j.dyepig.2022.110853.
[37] M. Gao, Y. Tian, J. Yang, X. Li, M. Fang, Z. Li, J. Mater. Chem. C 9 (2021) 15375–15380, https://doi.org/10.1039/D1TC03460J.
[38] Z. He, W. Li, G. Chen, Y. Zhang, W.-Z. Yuan, Chin. Chem. Lett. 30 (2019) 933–936, https://doi.org/10.1016/j.cclet.2019.03.015.
[39] S. Ito, CrystEngComm 24 (2022) 1112–1126, https://doi.org/10.1039/D1CE01614H.
[40] Q. Li, Z. Li, Acc. Chem. Res. 53 (2020) 962–973, https://doi.org/10.1021/acs.accounts.0c00060.
[41] S.K.B. Mane, Y. Mu, E. Ubba, Z. Yang, J. Zhao, Z. Chi, J. Mater. Chem. C 7 (2019) 15219–15224, https://doi.org/10.1039/C9TC05491J.
[42] O.W. Morawski, J. Karpiuk, M. Grzybowski, ChemPhysChem 25 (2024) e202400457, https://doi.org/10.1002/cphc.202400457.
[43] J. Wang, Z. Chai, J. Wang, C. Wang, M. Han, Q. Liao, A. Huang, P. Lin, C. Li, Q. Li, Z. Li, Angew. Chem. Int. Ed. 58 (2019) 17297–17302, https://doi.org/10.1002/anie.201911648.
[44] J. Zhang, M. Zhu, Y. Lu, X. Zhang, S. Xiao, H. Lan, T. Yi, Chem. Eur. J. 28 (2022) e202200458, https://doi.org/10.1002/chem.202200458.
[45] Y. Wang, Z. Zhang, L. Liu, S. Yuan, J. Ma, D. Liu, S. Xue, Q. Sun, W. Yang, J. Mater. Chem. C 7 (2019) 9671–9677, https://doi.org/10.1039/C9TC03444G.
[46] Z. Wu, Z. Xu, D. Wang, G. Deng, S. Lin, Z. Zhao, D. Wang, Y. Xiong, B.Z. Tang, Adv. Funct. Mater., n/a, 2415285. ⟨https://doi.org/10.1002/adfm.202415285⟩.
[47] E. Lucenti, A. Forni, C. Botta, L. Carlucci, C. Giannini, D. Marinotto, A. Previtali, S. Righetto, E. Cariati, J. Phys. Chem. Lett. 8 (2017) 1894–1898, https://doi.org/10.1021/acs.jpclett.7b00503.
[48] E. Cariati, A. Forni, E. Lucenti, D. Marinotto, A. Previtali, S. Righetto, C. Botta, V. Bold, V. Kravtsov, M.S. Fonari, Chem. Asian J. 14 (2019) 853–858, https://doi.org/10.1002/asia.201801604.
[49] E. Cariati, E. Lucenti, A. Previtali, A. Forni, Cyclic triimidazole derivatives: an intriguing family of multifaceted emitters, in: Handbook of Aggregation-induced Emission: Typical Aiegens Design, 2022, pp. 165–193.
[50] M.S. Fonari, V.C. Kravtsov, V. Bold, E. Lucenti, E. Cariati, D. Marinotto, A. Forni, Cryst. Growth Des. 21 (2021) 4184–4200, https://doi.org/10.1021/acs.cgd.1c00459.
[51] M. Formenti, D. Blasi, E. Cariati, L. Carlucci, A. Forni, C. Giannini, M. Guidotti, S. Econdi, D. Malpicci, D. Marinotto, E. Lucenti, Dyes Pigments 206 (2022) 110637, https://doi.org/10.1016/j.dyepig.2022.110637.
[52] E. Lucenti, E. Cariati, A. Previtali, D. Marinotto, A. Forni, V. Bold, V.C. Kravtsov, M. S. Fonari, S. Galli, L. Carlucci, Cryst. Growth Des. 19 (2019) 1567–1575, https://doi.org/10.1021/acs.cgd.8b01199.
[53] E. Lucenti, A. Forni, C. Botta, L. Carlucci, C. Giannini, D. Marinotto, A. Pavanello, A. Previtali, S. Righetto, E. Cariati, Angew. Chem. Int. Ed. 56 (2017) 16302–16307, https://doi.org/10.1002/anie.201710279.
[54] E. Lucenti, A. Forni, C. Botta, C. Giannini, D. Malpicci, D. Marinotto, A. Previtali, S. Righetto, E. Cariati, Chem. Eur. J. 25 (2019) 2452–2456, https://doi.org/10.1002/chem.201804980.
[55] E. Lucenti, A. Forni, A. Previtali, D. Marinotto, D. Malpicci, S. Righetto, C. Giannini, T. Virgili, P. Kabacinski, L. Ganzer, U. Giovanella, C. Botta, E. Cariati, Chem. Sci. 11 (2020) 7599–7608, https://doi.org/10.1039/d0sc02459g.
[56] D. Malpicci, A. Forni, C. Botta, C. Giannini, E. Lucenti, D. Marinotto, D. Maver, L. Carlucci, E. Cariati, Dyes Pigments 215 (2023) 111274, https://doi.org/10.1016/j.dyepig.2023.111274.
[57] D. Malpicci, A. Forni, C. Botta, C. Giannini, E. Lucenti, D. Marinotto, D. Maver, L. Carlucci, E. Cariati, Chem. Eur. J. 29 (2023) e202300930, https://doi.org/10.1002/chem.202300930.
[58] D. Malpicci, E. Lucenti, A. Forni, D. Marinotto, A. Previtali, L. Carlucci, P. Mercandelli, C. Botta, S. Righetto, E. Cariati, Inorg. Chem. Front. 8 (2021) 1312–1323, https://doi.org/10.1039/d0qi01377c.
[59] E. Melnic, V.C. Kravtsov, E. Lucenti, E. Cariati, A. Forni, N. Siminel, M.S. Fonari, New J. Chem. 45 (2021) 9040–9052, https://doi.org/10.1039/d1nj00909e.
[60] A. Previtali, W. He, A. Forni, D. Malpicci, E. Lucenti, D. Marinotto, L. Carlucci, P. Mercandelli, M.A. Ortenzi, G. Terraneo, C. Botta, R.T.K. Kwok, J.W.Y. Lam, B. Z. Tang, E. Cariati, Chem. Eur. J. 27 (2021) 16690–16700, https://doi.org/10.1002/chem.202102839.
[61] E. Lucenti, A. Forni, C. Botta, L. Carlucci, A. Colombo, C. Giannini, D. Marinotto, A. Previtali, S. Righetto, E. Cariati, ChemPhotoChem 2 (2018) 801–805, https://doi.org/10.1002/cptc.201800151.